

**Numerical Simulations for Dynamical Universality Classes
Without Time-Reversal Symmetry**

by

Henry Waldstreicher

A thesis submitted to the
Faculty of the Graduate School of the
University of Colorado in partial fulfillment
of the requirements for the degree of
Bachelor of Arts
Department of Physics
April 10, 2023

Committee Members:

Dr. Andrew Lucas, Thesis Advisor, Department of Physics, Chair
Dr. Paul Beale, Honors Council Representative, Department of Physics
Dr. Jeanne Clelland, Outside Reader, Department of Mathematics

Waldstreicher, Henry (B.A., Physics)

Numerical Simulations for Dynamical Universality Classes Without Time-Reversal Symmetry

Thesis directed by Dr. Andrew Lucas, Thesis Advisor, Department of Physics

We present the simulation of Markov chains which can simulate kinematically constrained many-body dynamics. Our method gives Markov chains with a desired stationary distribution, and spatially local dynamics, while controllably breaking time-reversal symmetry. To break time-reversal symmetry we developed an algorithm that finds transitions that break detailed balance and transitions that maintain charge/dipole conservation, and then chooses which set of transitions will give the largest signal when simulated.

Contents

Chapter

1	Introduction	1
1.1	Hydrodynamics	1
1.2	Hydrodynamics with constrained kinematic motion	3
1.3	Breaking Time-Reversal Symmetry	5
2	Mathematical Justification	7
2.1	Markov Chains	7
2.2	Many Body Dynamics	10
2.3	Parity and Time-Reversal symmetry	11
3	Algorithm	14
3.1	Detailed Balance Breaking Transitions	14
3.2	Enforcing Conservation	17
3.3	Optimization	19
4	Numerical Results	21
4.1	Recovering previous results	21
4.2	Towards breaking time-reversal symmetry	22
5	Conclusion	25

Bibliography

Figures

Figure

1.1	Fick's law of diffusion in different media	3
1.2	KPZ scaling for sound mode of 1D Navier-Stokes[2]	5
2.1	Example microscopic transition matrix for $m=q=4$ with charge and dipole conserved. The blue to purple transition is: 2 charges on site 2 splitting and moving away from each other equally. the blue to red transition is: one charge at site 1 and one charge at site 2 moving away from each other equally. The blue to green transition is all charges moving 1 site away from site 2, half right and half left.	8
4.1	Results from previous literature [4]. b) is sub-diffusive results for $C(0, t)$ in dipole and quadrupole conserving fluids. c) shows scaling collapse according to the long wavelength description	21
4.2	Simulation for $m = 3, q = 5$ showing $C(0, t)$ giving $Z = 4$ sub-diffusive behavior	22
4.3	$C(x, t)$ correlation function following (4.1.1) and agreeing with Figure 4.1, finding the long wavelength description.	22
4.4	Null vector for $m = q = 2, n_{01} = -\frac{1}{\sqrt{2}}, n_{10} = \frac{1}{\sqrt{2}}$	22
4.5	a) Motifs corresponding to the vector entries. b) Null vectors for $m = 2, q = 3$. Each entry is the f value for the corresponding motif. Similarly to Figure 4.4, we can read the columns in (b) as the f values corresponding to the motif in the same row in (a). 001 can have an f value of -.596, .5 or .0958 etc.	23

- 4.6 Optimized vector for $m = 2$, $q = 3$. Each f value is underneath it's corresponding motif, so
001 has an f of -0.5963 etc. 23
- 4.7 \mathcal{T} breaking transition matrix for $m = q = 2$, the columns are ordered 00, 10, 01, 11 24

Chapter 1

Introduction

1.1 Hydrodynamics

If one were to place a drop of creamer into their coffee, they would see initially the creamer concentrated in one spatial region, and as time steps forward the creamer would blend into the coffee, eventually reaching an equilibrium when the solution is fully mixed. This behavior is called diffusion, and many different systems follow that same behavior. Tracking any individual particle would be incredibly complex and not very informative, since every individual molecule is strongly interacting with its environment in a very complicated way. However, over large time scales for some relatively large sample, we have a description of the dynamics of how the system reaches equilibrium. The effective theory that governs these dynamics is hydrodynamics.

An effective theory describes a set of behaviors that systems obey over large time and/or length scales. At these scales we are able to integrate the microscopic degrees of freedom out of our model. We use these equations to mathematically 'zoom out' and look at a system spatially or temporally to model and predict the emergent behavior. This 'zooming out' reduces the degrees of freedom for a system to just quantities that are conserved, like particle number, since every other type of degree of freedom (such as the velocity of a particle) quickly decays in a microscopic time scale associated with inter-particle collisions. Focusing only on the hydrodynamic, slow, degrees of freedom allows for feasible simulation of the dynamics.

The minimal theory of hydrodynamics is diffusion of a single conserved charge. For this case the

microscopic equation of motion is given by the continuity equation:

$$\partial_t \rho = -\nabla \cdot J \quad (1.1.1)$$

This minimal theory differs in scope from the traditional formulation of hydrodynamics, but the conceptual starting point is the same.

Traditionally called fluid mechanics, hydrodynamics looks at how water and other fluids move over a long time scale with sufficient samples. This traditional formulation asks questions like how does water flow through a pipe, or how does water flow in a waterfall. These classical questions have quantum analogs such as how do electrons flow through a constriction in graphene [12]. We have answers to the classical questions of hydrodynamics because we only look at long time scales, and due to that we only keep track conserved quantities like energy or momentum. These conserved quantities exist whether or not the microscopic dynamics are classical or quantum. If we can use a mechanical theory that doesn't depend on the nature of a system being quantum or classical, like statistical mechanics, to answer the classical questions of hydrodynamics, we should be able to use the same formulation to predict the hydrodynamic behaviors of quantum systems. For example, many classical fluids obey the Navier-Stokes equations, but the Navier-Stokes equations are not sensitive to microscopic details of the particles themselves. The example of electrons flowing through a constriction in graphene is a quantum fluid that is observed to obey the Navier-Stokes equations. [12]

In the modern formulation of hydrodynamics, we study how some complex many body system thermalizes, or achieves thermal equilibrium. This question involves foundational principles of physics, and ultimately allows us to model “simple” questions about how fluids move around obstacles. Importantly, we look at **why** fluids thermalize the way they do, rather than focusing on peculiarities of a particular experimental geometry, boundary conditions, or initial conditions to describe how a fluid moves. Diffusion can be described using Fick's laws where ρ is the density of the single conserved quantity and J is the conserved current or diffusive flux: the amount of substance that will diffuse through a unit area:

$$J_i = -D\partial_i \rho \quad (1.1.2)$$

Combining with the continuity equation (1.1.1) we find

$$\partial_t \rho = D\partial_x^2 \rho \quad (1.1.3)$$



(a) Mass transfer diffusion example [10]

(b) Self Diffusion of toluene example [5]

Figure 1.1: Fick's law of diffusion in different media

This scaling occurs anywhere there is diffusion with a single conserved quantity, so mass transfer[10], toluene vapor diffusion[5], and conserved charges diffusing all obey this scaling at hydrodynamic time scales. Using dimensional analysis we can say that

$$\frac{[\rho]}{time} \sim \frac{[\rho]}{length^2} \quad (1.1.4)$$

$$length^2 \sim time \quad (1.1.5)$$

$$x^2 \sim t \quad (1.1.6)$$

so our relaxation time, or the time to reach equilibrium, scales quadratically with our system size. Saying that all of these systems obey the same hydrodynamic scaling is another way of saying they all exist in the same **universality class**. A universality class is a collection of dynamical systems that asymptotically have the same behavior.

1.2 Hydrodynamics with constrained kinematic motion

This thesis discusses the universality classes arising from kinematically constrained fluids. A kinematic constraint means there is some microscopic restriction on the local mobility of individual particles, so a subset of the degrees of freedom are unavailable. People experience this kind of constraint daily when driving. A car can move freely in $2D$ but should only go forward or backward on a one lane road.

Kinematically constrained fluids, dubbed fracton fluids, belong to new hydrodynamic universality classes [6]. The kinematic constraint we are exploring is the conservation of the dipole moment. Adding this conserved quantity changes (1.1.3) by requiring $\partial_t \int dx x \rho = 0$, or that the dipole moment ($\int dx x \rho$) doesn't

change with time.

$$\partial_t \int dx x \rho = \int dx x \partial_t \rho \quad (1.2.1)$$

$$= - \int dx x \partial_x J_x \text{ by the continuity equation 1.1.1} \quad (1.2.2)$$

$$= \int dx J_x \text{ after integrating by parts} \quad (1.2.3)$$

Our boundary values vanish because we are considering dynamics with periodic boundary conditions. (1.2.3)

only vanishes if $J_x = \partial_x J_{xx}$, so we obtain $\partial_t \rho + \partial_x J_x = \partial_t \rho + \partial_x^2 J_{xx} = 0$. This gives [8]

$$\partial_t \rho = -B \partial_x^4 \rho \quad (1.2.4)$$

since with time reversal symmetry

$$J_{xx} = B \partial_x^2 \rho \quad (1.2.5)$$

where J_{xx} is the symmetric dipole current. In ideal hydrodynamics, lowest order with no derivatives in the current, time-reversal symmetry must be respected. Importantly, the sub-diffusive result arises because we cannot write J_{xx} as a function of ρ [8], we must use derivatives of ρ . This is because fractons are an isotropic fluid, meaning they exhibit the same properties regardless of the direction of measurement. Being homogeneous and isotropic means we have spatial and temporal inversion symmetry [3]. The nature of J_{xx} being time reversal odd then forces only derivatives of ρ , a time reversal even function, to appear since time reversal symmetry is not broken in ideal hydrodynamics. The existence and conservation of this dipole moment adds another conserved quantity that constrains how particles move around the system as thermalization occurs, so a sub-diffusive scaling ($t \sim x^4$) is sensible. This sub-diffusive scaling has been verified experimentally with cold atoms in a tilted atomic lattice [7].

This relationship between J_{xx} and ρ begs the question: is hydrodynamics stable to fluctuations? Given that J_{xx} is time-reversal odd and ρ is time-reversal even, we can explore hydrodynamic stability by controllably breaking time-reversal symmetry.

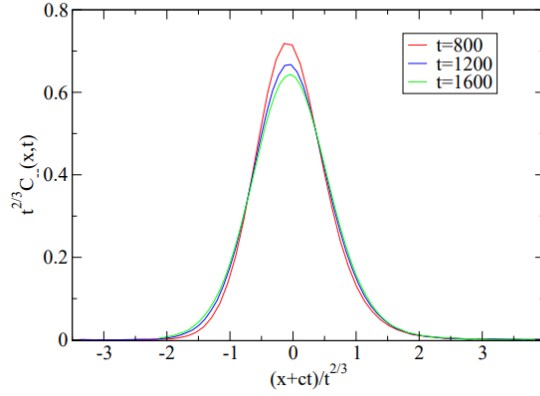


Figure 1.2: KPZ scaling for sound mode of 1D Navier-Stokes[2]

1.3 Breaking Time-Reversal Symmetry

Why do we want to introduce instability by breaking time-reversal symmetry? In classical fluids, hydrodynamics is unstable to fluctuations in 1D. If we take a quadratic perturbation in the density term of the 1D Navier-Stokes equations, rather than finding the Gaussian fixed point, the endpoint of the dynamics actually belongs to the Kardar-Parisi-Zhang (KPZ) universality class [9]. As an example, if we look at a 1D chain of interacting particles and take correlation functions of the density, the correlation function is **not** given by a solution to the hydrodynamic PDEs. A correlation function is an expectation value of a product of two variables separated by time or space. We see this in Figure 1.2.

In this thesis we want to understand the breaking of time-reversal symmetry to learn whether new Kardar-Parisi-Zhang-like dynamical universality classes can arise in this theory. We can visualize time-reversal symmetry by imagining a video of some dynamics. If we were to rewind the video and not be able to tell, then those dynamics are time-reversal symmetric. Immediately, the idea of a time reversible diffusive system might cause alarm, dye mixing with water does not look like dye being removed from water. This diffusive behavior because there are more water/dye mixed states than unmixed states, but every possible configuration is equally likely. This means that any transition from a state looks like any transition back into that state, so the video looks the same playing forward and backward. The dynamics in this example are modeled by the transitions between microscopic states of the system, or microstates.

Thermal systems that obey this same behavior are subject to the fluctuation-dissipation theorem, and Kubo-Martin-Schwinger (KMS) symmetry generates time-reversal symmetry for dissipative thermal systems [1]. Our formulation uses systems that obey detailed balance, and transformations that look like KMS symmetry [8], so even in our non-thermal dissipative system we have a reasonable notion of time-reversal symmetry.

With this notion of time-reversal symmetry, we can controllably break it by emulating a biased random walk. A biased random walk is a walk on a graph where the probability to transition to any state is not uniform, there are some preferred transitions. When we say controllably, in this context we mean that our system is constructed such that we control how large a bias we implement

We will do this through specific construction of Markov chains that break detailed balance but maintain stationarity.

Chapter 2

Mathematical Justification

To provably break time-reversal symmetry, we need to construct a Markov chain with preferred transitions that still has some known distribution of states to relax to.

2.1 Markov Chains

A brief note on notation: \mathbf{Q} represents a matrix and we represent column vectors as $|x\rangle$. We use this bra-ket notation because it is elegant, not because our model involves quantum mechanics. Our model and all simulations are classical.

First we define a global probability distribution:

$$|\mathbf{P}\rangle = \sum_x P_x |x\rangle = \sum_x P(x) |x\rangle \quad (2.1.1)$$

Using this probability distribution, we can evolve our system by locally updating some q consecutive sites and transitioning with some probability, $P(x)$. These transitions are stochastic, and we can describe this behavior using a Markov chain. Now we can define our transition matrix, \mathbf{Q}

$$Q^{gate} = \sum_y Q_i^{gate}(x \rightarrow y) |y\rangle \langle x| \text{ for } i \leq L \quad (2.1.2)$$

A Markov chain is a stochastic process in which the future state of the system depends only on the present state, satisfying the Markov condition. Schematically this means that we must construct stochastic transition matrices, which have all columns summing to 1. The chains are made of every possible state that a system can exist in, and each state has some associated probability to transition in and out (P_{in} and P_{out}). We model

charge/dipole conserving dynamics by having each transition be an allowed move of particles, which must move with other particles. The dipole constraint forces charges to move away from each other symmetrically, or for +- charge pairs to always move together. Every possible transition is one allowed move of charges (described explicitly in Figure 2.1). Since every state in a given sector can be transitioned into/out of we say that all states **communicate** and are **essential**. This combination implies they exist in a unique essential communicating class, which guarantees the existence of at least one stationary distribution[11]. The **stationary distribution**, denoted $|\pi\rangle$, describes the distribution of states once the Markov chain is done evolving through time. Formally The stationary distribution is a +1 eigenstate of Q:

$$|\pi\rangle = Q|\pi\rangle \quad (2.1.3)$$

Equivalently, an elementwise formulation gives

$$\pi(y) = \sum_x \pi(x)P(x,y) \quad (2.1.4)$$

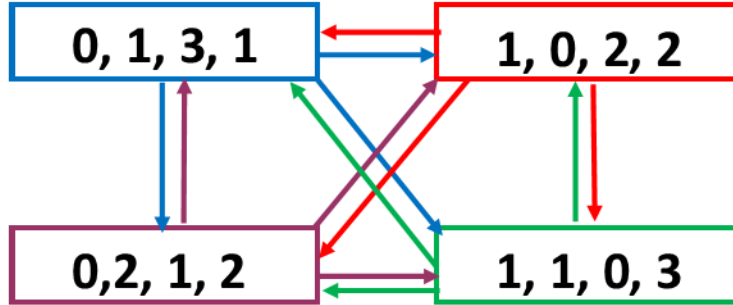


Figure 2.1: Example microscopic transition matrix for $m=q=4$ with charge and dipole conserved. The blue to purple transition is: 2 charges on site 2 splitting and moving away from each other equally. the blue to red transition is: one charge at site 1 and one charge at site 2 moving away from each other equally. The blue to green transition is all charges moving 1 site away from site 2, half right and half left.

Figure 2.1 is a microscopic chain for a transition of our systems, and it shows 2 important properties

of our Markov chains. First, we see that every state in this microscopic chain communicates with each other, i.e every state can transition to every other state. This makes every state essential and means that they are all part of one unique essential communicating equivalence class. This also means that this microscopic chain is **irreducible**, meaning that we cannot remove some collection of states from the chain without affecting the transition probabilities. The second is that the $P_{in} = P_{out}$ for all states, creating a uniform stationary distribution.

Another important property of Markov chains is **detailed balance**. The detailed balance equation is

$$\hat{Q}(x, y) \equiv \frac{\pi(y)Q(y, x)}{\pi(x)} \quad (2.1.5)$$

and tells us that when a Markov Chain obeys detailed balance, time reversed chain is equal to the original. We call $\hat{Q}(x, y)$ the time-reversed chain of $Q(y, x)$. A Markov Chain that obeys detailed balance, then, has **time-reversal symmetry** denoted \mathcal{T} . If $|\pi|$ is uniform then (2.1.5) requires that Q is symmetric. If Q is symmetric, we can also say that $P_{in} = P_{out}$ for all states.

Let us more explicitly define some properties of the states of our Markov chain. We can define an essential state as, for finite chains a state x is essential if and only if [11]

$$Q_x\{\tau_x^+ < \infty\} = 1 \quad (2.1.6)$$

Where τ_x^+ is the **hitting time**, or the time it takes for the chain to first visit x , so if some state x has a probability of 1 to be hit before $t = \infty$ then x is essential. If a state in a finite chain satisfies (2.1.6) then it is **recurrent**.

Next, we say that x **communicates** with y if and only if $x \rightarrow y$ and $y \rightarrow x$, and we write that as $x \leftrightarrow y$. The equivalence classes for these relations are called **communicating classes**. For an irreducible chain there is only one equivalence class. Communicating classes can be essential if all states within them are essential, we call these **essential communicating classes**.

Proposition 1.29 in [11] says that the transition matrix Q has a unique stationary distribution if and only if there is a unique essential class, and if there are distinct essential classes Q has at least one stationary distribution.

2.2 Many Body Dynamics

To simulate hydrodynamics using Markov chains we need to ensure the existence of a stationary distribution so that we can sample the equilibrium correlation functions, as that will determine the universality class. This initially creates a problem because our Markov chain is reducible, and reducible chains are not guaranteed a stationary distribution. This, however, is solved by our construction.

We simulate hydrodynamics by randomly swapping q -gates with other configurations of charges with the same charge and dipole moment. Remember that this random swapping represents possible movements of the charges according to the kinematic constraint. This creates unique essential communicating classes and as per the discussion in Section 2.1 means that there exists a unique stationary distribution. Since the transition is uniform inside the communicating classes, the transition matrix inside each communicating class is doubly stochastic. After normalizing the sum of every communicating class transition matrix the \mathbf{Q} for the fully symmetric system is doubly stochastic and so $|\pi\rangle$ is uniform.

We are creating these 1D Markov chains with periodic boundary conditions. Each site can have a charge of $0, 1, \dots, m-1$. We update q sites locally in each time step. We define the total charge for a state as the sum of all charges in that state, and the total dipole moment as $\sum_{x=1}^q x\rho[x]$ where $\rho[x]$ is the charge at site x . From these initial conditions we are interested in the behavior of gates with q sequential sites inside them called q -gates. For Figure 2.1 our $m = q = 4$, so we look for sets of 4 sequential sites where each site can have charge 0, 1, 2, or 3, and where all q -gates only update to q -gates with the same charge and dipole moment. Requiring all allowed transitions to have the same charge and dipole creates communicating classes within those sectors. In this full symmetry case each transition inside the communicating classes looks like the figure, so every state is essential and every communicating class is unique and essential. From the previous section we know that this guarantees the existence of at least one stationary distribution. This is vital because we have m^L total microstates, $|x\rangle$ so our state space is exponential in L .

We can construct a local \mathbf{Q}_i^{gate} such that we have a stochastic process since the transition must occur, and our states are essential. Since we only want to act on one q -gate at a time, we enforce spatial locality. Locality refers to the principle that physical interactions can only occur at points in space-time that are

close to each other, so in our case we define close to be within the q -gate. This is a fundamental postulate for physics and hydrodynamics. Globally we can describe acting on an individual arbitrary state $|x\rangle$ with:

$$\mathbf{Q}_i^{gate} = \mathbf{1}_1 \otimes \mathbf{1}_2 \otimes \cdots \otimes \mathbf{1}_{i-1} \otimes \mathbf{Q}_i^{gate} \otimes \mathbf{1}_{i+q} \otimes \cdots \otimes \mathbf{1}_L \text{ for } i + q \leq L \quad (2.2.1)$$

where every operator acts on a q -gate. From here we are looking for the average trajectory of the multiple transition matrices we use to act \mathbf{Q} on the entire state rather than one q -gate, so we look at the classical probability of selecting some gate j out of a total of L gates. Then we can rewrite \mathbf{Q} as

$$\mathbf{Q} = \sum_{j=1}^L \frac{1}{L} \mathbf{Q}_j^{gate} \quad (2.2.2)$$

So

$$\sum_y \mathbf{Q}(x \rightarrow y) = \sum_{j=1}^L \frac{1}{L} \mathbf{Q}_j^{gate}(x \rightarrow y) = \frac{1}{L} L = 1 \quad (2.2.3)$$

where now we can have a stochastic transition matrix \mathbf{Q} acting globally. Note that we are assuming periodic boundary conditions on the microstates.

$$j \cong j + L \quad (2.2.4)$$

2.3 Parity and Time-Reversal symmetry

We are interested in exploring the time reversal symmetry (\mathcal{T}) and parity symmetry (\mathcal{P}) of our Markov chains. We looked at the time reversed transition matrix in the detailed balance discussion (2.1.5). Parity symmetry is defined as $\mathbf{Q} = \Pi \mathbf{Q} \Pi^{-1}$ for some operator Π and can be interpreted as the system behaving the same if we label $j \rightarrow -j$. This is simply changing the basis of our \mathbf{Q} , so conjugation by Π where Π flips the sign of j describes the transformation. A symmetry is a transformation that leaves the equation of motion invariant (if it is obeyed), and the 'equations of motion' in our model are the transition probabilities in \mathbf{Q} .

Now the question is what can guarantee with specific construction when we want to break \mathcal{T} ?

As an example, we can break \mathcal{T} by constructing a biased random walk that biases towards moving charge to the right. To build this transition matrix we are creating two local transition matrices, a \mathcal{T} broken transition matrix and a transition matrix with both \mathcal{P} and \mathcal{T} , and adding them together. We can then construct a macroscopic transition matrix by combining our local microscopic transition matrices. A simple

example is with charge conservation and $m = q = 2$. In this example our motifs are: 00, 01, 10, and 11 so to bias right 10 and 01 both must prefer transitioning to 01.

$$\mathbf{Q}_{local} = \begin{array}{c} \begin{array}{cccc} & 00 & 01 & 10 & 11 \\ \begin{array}{c} 00 \\ 01 \\ 10 \\ 11 \end{array} & \begin{pmatrix} \frac{1}{2} & 0 & 0 & 0 \\ 0 & \frac{1}{4} & \frac{1}{4} & 0 \\ 0 & \frac{1}{4} & \frac{1}{4} & 0 \\ 0 & 0 & 0 & \frac{1}{2} \end{pmatrix} & + & \begin{array}{cccc} & 00 & 01 & 10 & 11 \\ \begin{array}{c} 00 \\ 01 \\ 10 \\ 11 \end{array} & \begin{pmatrix} \frac{1}{2} & 0 & 0 & 0 \\ 0 & \frac{1}{2} & \frac{1}{2} & 0 \\ 0 & 0 & 0 & 0 \\ 0 & 0 & 0 & \frac{1}{2} \end{pmatrix} \end{array} \end{array} \quad (2.3.1)$$

$$= \begin{pmatrix} 1 & 0 & 0 & 0 \\ 0 & \frac{3}{4} & \frac{3}{4} & 0 \\ 0 & \frac{1}{4} & \frac{1}{4} & 0 \\ 0 & 0 & 0 & 1 \end{pmatrix} \quad (2.3.2)$$

for some state $|x\rangle$. This example shows a combination of the 0, 1, and 2 total charge sector microscopic transition matrices. In this example we see that 01 is biased over 10, but 10 can still appear. The addition of these transition matrices guarantees that the hitting time of any state obeys (2.1.6) since there is always a probability to transition into and out (P_{in}, P_{out}) of any given state. This maintains our equivalence class and thus the existence of our stationary distribution. We need to maintain the existence of a known stationary distribution because our state space grows exponentially with the system size, m^L , and we cannot sample from every state for large systems. It is important to note that these transition probabilities include self transitions. Furthermore, we ensure that $P_{in} = P_{out}$ for each equivalence class. If \mathbf{Q}^{gate} is symmetric, or obeys \mathcal{T} then this result is trivial. We can prove that our construction guarantees this condition generally with the following:

Let \mathbf{Q} be the transition matrix from x for all y , and $P(x, y)$ be the probability of $x \rightarrow y$ for a given y .

$$P(x, y) = \delta_{xy}[1 - \sum_{y, y \neq x} Q_{yx}] + Q_{yx} \quad (2.3.3)$$

$$\pi_{eq}(x)P(x, y) = \pi_{eq}(x)(\delta_{xy}[1 - \sum_{y, y \neq x} Q_{yx}] + Q_{yx}) \quad (2.3.4)$$

$$\sum_x \pi_{eq}(x)P(x, y) = \sum_x \pi_{eq}(x)(\delta_{xy}[1 - \sum_{y, y \neq x} Q_{yx}] + Q_{yx}) \quad (2.3.5)$$

We can rewrite using (2.1.4) as

$$\pi_{eq}(y) = \sum_x \pi_{eq}(x)\delta_{xy}[1 - \sum_{y, y \neq x} Q_{yx}] + \pi_{eq}(x)Q_{yx} \quad (2.3.6)$$

$$= \sum_x \pi_{eq}(x)\delta_{xy} - \sum_x \delta_{xy}\pi_{eq}(x) \sum_{y, y \neq x} Q_{yx} + \sum_x \pi_{eq}(x)Q_{yx} \quad (2.3.7)$$

$$= \pi_{eq}(y) - \pi_{eq}(y) \sum_{x, y \neq x} Q_{xy} + \sum_x \pi_{eq}(x)Q_{yx} \quad (2.3.8)$$

$$0 = \sum_x [\pi_{eq}(y)Q_{xy} - \pi_{eq}(x)Q_{yx}] \quad (2.3.9)$$

$$\sum_x \pi_{eq}(y)Q_{xy} = \sum_x \pi_{eq}(x)Q_{yx} \quad (2.3.10)$$

$$P_{out} = P_{in} \quad (2.3.11)$$

Now we have a stationary distribution which we can sample from, and our $P_{in} = P_{out}$ so we know that our stationary distribution is uniform.

Chapter 3

Algorithm

How do we create these transition matrices that have some preferred transition, break detailed balance, yet still guarantee the existence of a uniform stationary distribution and maintain charge/dipole conservation? We developed an algorithm that 1) finds the transitions that break detailed balance, 2) finds the transitions that maintain charge/dipole conservation, 3) finds the intersection of those sets, and 4) chooses the set of transitions that creates the largest signal.

3.1 Detailed Balance Breaking Transitions

To properly understand our algorithm it is easiest to start with what we are emulating. We are turning a uniform random walk into a biased random walk. This creates some set of preferred transitions that do not behave identically with time flowing forward or backward, breaking time reversal symmetry. We do this by recognizing that, for $q = m = 2$ the number of 10 q -gates must equal the number of 01 q -gates, so we can bias moving charges right by enforcing that 10 and 01 prefer to transition to 01. If we transition from 10 to 01 and then reverse time while maintaining our update rules, 01 will transition to 01 not back to 10, breaking \mathcal{T} . For small systems we can exhaustively see these update rules, but how can we explore larger systems? We can exploit the fact that, like with small systems, certain sets of q -gates must have the same number of occurrences. The problem then is to find these sets of q -gates.

Let's start with the inherent properties of our system. All of our systems have periodic boundary conditions, so $x \sim x + L$, and we want to locally conserve charge and dipole moment. Forcing local conservation of these quantities locks our system into only transitioning to microstates within the same

charge and dipole sector. We define q_x as the charge on some site, x , and $f(q_i)$ as arbitrary functions. This allows us to write:

$$\sum_{x=1}^L f(q_x) = \sum_{x=1}^L f(q_{x+1}) \quad (3.1.1)$$

$$\sum_{x=1}^L f(q_x) - f(q_{x+1}) = 0 \quad (3.1.2)$$

$$\sum_{x=1}^L f(q_x, q_{x+1}) = 0 \text{ where } f(q_x, q_{x+1}) = f(q_x) - f(q_{x+1}) \quad (3.1.3)$$

Periodic boundary conditions and conservation of charge/dipole give us (3.1.1), as it doesn't matter where in the system we start the sum if we sum over every index. This now becomes a question of what are the allowed $f(q_x)$? We first define $f_k(q) = q^k$ for $j, k \in \{0, 1, \dots, m-1\}$. Trivially, if $k = 0$ then $f_0(q_x, q_{x+1})$ must be identically 0, but can we find a nontrivial function for larger k ? We can answer this by walking through an example with $m = q = 2$. With these constraints our only potential nontrivial function is $f_1(q) = q$, so we have

$$\sum_{x=1}^L q_x = \sum_{x=1}^L q_{x+1} \quad (3.1.4)$$

$$\sum_{x=1}^L q_x - q_{x+1} = 0 \quad (3.1.5)$$

Our only q -gates are 00, 01, 10, and 11. We can see that $f(0, 0) = 0 - 0$ and $f(1, 1) = 1 - 1$ so 11 and 00 don't contribute to the sum. We are left with $f(1, 0) = 1$ and $f(0, 1) = -1$, and this gives us what we need to find the preferred transitions. (3.1.5) tells us that if there is more charge on the right our function will have a negative value for that motif. Moreover, for (3.1.3) to be true then there must be an equal number of motifs that shift charges left, giving a positive value. In this example we find $n_{01} = n_{10}$. What are some transitions on the entire microstate ($L = 4$) that maintain this added constraint? The first is bit-flipping neighboring sites.

$$n_{01} = 1 = n_{10}, 0100 \rightarrow 0010, n_{01} = 1 = n_{10}$$

$$n_{01} = 1 = n_{10}, 1001 \rightarrow 1010, n_{01} = 2 = n_{10}$$

$$n_{01} = 1 = n_{10}, 1100 \rightarrow 0101, n_{01} = 2 = n_{10}$$

Similarly, only flipping one bit maintains this added constraint. However, this single bit flip **violates** charge conservation, so we will have to impose another constraint to maintain our conservation rules in the final update rules.

$$n_{01} = 0 = n_{10}, 0000 \rightarrow 0100, n_{01} = 1 = n_{10}$$

$$n_{01} = 1 = n_{10}, 0100 \rightarrow 0110, n_{01} = 1 = n_{10}$$

Immediately, if we can find these transitions by observation and some simple check-sums then why are these f's useful? The issue is that all of these transitions are guaranteed by detailed balance and a uniform stationary distribution. If we act the bit-flipping operator twice on 0000 it will return 0000. However, if we enforce \mathcal{T} breaking updates these transitions are not guaranteed. Looking back at the non-trivial function we found, we must ensure that we maintain $P_{in} = P_{out}$ and $\sum_x f_x = 0$. Since we bias charges to the right, we identify $P_{in} = \lambda n_{01}$ and $P_{out} = \lambda n_{10}$ where λ is a normalization factor. We then see

$$\sum_x f_x = (n_{01} - n_{10}) \tag{3.1.6}$$

$$= P_{in} - P_{out} = 0 \tag{3.1.7}$$

$$P_{out} = P_{in} \tag{3.1.8}$$

(3.1.8) shows that a transition that breaks detailed balance also maintains the existence of a stationary distribution. We argue that the f's show us what transitions break \mathcal{T} while maintaining stationarity.

We can generalize this $L = q = 2$ case to arbitrary L and q . Consider the family of functions

$$f_x^q = f(q_x, q_{x+1}, \dots, q_{j+q-1}) \tag{3.1.9}$$

$$\propto (q_x^{k_x} q_{x+1}^{k_{x+1}} \dots q_{x+q-1}^{k_{x+q-1}} - f_{translate}(j)) \tag{3.1.10}$$

Where $f_{translate}(q)$ is a translational term owing to the periodic boundary conditions of our system. (3.1.10) enforces

$$\sum_j f_j^q = 0 \tag{3.1.11}$$

For an arbitrary f_j we say

$$P_{in} \propto \sum_j f_j \Theta[f_j] \quad (3.1.12)$$

$$P_{out} \propto \sum_j (-f_j) \Theta[-f_j] \quad (3.1.13)$$

Where $\Theta[x]$ is a Heaviside function. Rather than compute these sums outright, we recognize that since the preferred motifs always appear with the same frequency as the unpreferred motifs a computation of the null vector in the motif frequency basis suffices.

$$\vec{N} = (n_{00\dots 0}, n_{00\dots 1}, \dots, n_{mm\dots m}) \quad (3.1.14)$$

$$\vec{c} \cdot \vec{N} = 0 \quad (3.1.15)$$

Where, up to normalization, the values in \vec{c} are the $f_j(\vec{s})$ values for the corresponding motif \vec{s} . For $m = q = 2$ the \vec{c} is $(0, -1, 1, 0)$, where the negative values indicate a transition **into** that motif and the positive values indicate a transition **out** of that motif. Our constraints limit the amount of allowed functions f , so that for a general system there are $m^{q-1} - 1$ possible f 's, and each f corresponds to a unique set of transition rules. A full proof of the $m^{q-1} - 1$ result will be presented in future work, but our numerical simulations always find $m^{q-1} - 1$ null vectors so we can be reasonably confident in this rule. To find all of the null vectors in practice we numerically generate a matrix of \vec{N}_i where $k \geq m^{q-1} - 1$

$$\begin{pmatrix} \vec{N}_0 \\ \vec{N}_1 \\ \vdots \\ \vec{N}_k \end{pmatrix}$$

and find the null space, \mathbf{C} . This gives all possible update rules, but we need to ensure that we are using update rules that conserve our desired symmetries.

3.2 Enforcing Conservation

If we remember the possible transitions that break detailed balance but maintain the $n_{10} = n_{01}$ constraint, there were a subset of transitions that broke charge/dipole conservation as well. Thus, we need

to enforce charge/dipole conservation on our possible preferred motifs, so that we are only swapping between states that have the same charge and dipole moment. We can accomplish this by creating charge/dipole projectors, that zero out the transitions that break these conservation rules. We create these projectors using $\mathbf{P} = \mathbf{1} - \mathbf{M}$ where, for each $N \times N$ block of states with the same charge and dipole moment \mathbf{M} has uniform entries $\frac{1}{N}$. This creates a null projector that eliminates transitions that do not stay within the charge and dipole block.

As an example, let us look at charge conservation in $m = q = 2$.

$$\mathbf{M} = \begin{array}{cc} & \begin{array}{cccc} 00 & 01 & 10 & 11 \end{array} \\ \begin{array}{c} 00 \\ 01 \\ 10 \\ 11 \end{array} & \left(\begin{array}{cccc} 1 & 0 & 0 & 0 \\ 0 & .5 & .5 & 0 \\ 0 & .5 & .5 & 0 \\ 0 & 0 & 0 & 1 \end{array} \right) \end{array}$$

so the full projector is then

$$\mathbf{P} = \mathbf{1} - \mathbf{M} = \left(\begin{array}{cccc} 0 & 0 & 0 & 0 \\ 0 & .5 & -.5 & 0 \\ 0 & -.5 & .5 & 0 \\ 0 & 0 & 0 & 0 \end{array} \right)$$

We can check that this result is a projector by checking if it is idempotent, $\mathbf{P}^2 = \mathbf{P}$. In this example we find that 00 and 11 cannot transition, and $01 \leftrightarrow 10$. for this size the detailed balance breaking transitions are a subset of the symmetry preserving transitions. Of course, this symmetry conservation restriction further decreases the number of possible transitions.

To find all of the transitions that both break detailed balance and obey the desired conservation laws, we want to find the intersection of our vector spaces. One way to find the intersection of these vector spaces by taking the singular value decomposition (SVD) of

$$P_{dipole} \mathbf{C} P_{dipole} = U \Sigma V^\dagger$$

In this decomposition, the rows of U are vectors that are in the union of our two vector spaces. Any row of

U that corresponds to a singular value of 1 in Σ is a vector in the intersection of our vector spaces.

3.3 Optimization

Once we've extracted all vectors with a singular value of 1, we need to decide which set of update rules will give the largest signal. To do this, we will again start by discussing the simplest case, where we are just conserving charge. We still want to break \mathcal{T} by moving charges to the right more often than to the left, and we can measure charge movement by calculating the average increase in the dipole moment after an update. If an update to some state \vec{s} increases the dipole moment of \vec{s} , then the charges in that state must have moved to the right on average. This behavior is governed by $\partial_t \rho = \partial_x \rho$. Using our example walk from before with $q = m = 2$ where 01 and 10 bias towards transitioning to 01, the dipole moment tends to increase from 1 to 2 or stay at 2, the maximum value. In this example we find:

$$\partial_t \int dx x \rho = \int dx x \partial_t \rho = \int dx x \partial_x \rho = - \int dx \rho \quad (3.3.1)$$

which is always a positive value because ρdx is either -1 (1 swaps with a 0) or 0 (nothing happens). When we want to extend this argument to preserve charge and dipole moment, we must increase the octopole moment.

We can't maximize over the dipole moment because that is conserved, and if we maximize over the quadrupole moment ($\int dx x^2 \rho$) we find dissipative behavior in the hydrodynamic description ($\partial_t \rho \sim \partial_x^2 \rho$) [8]. We also know that $J_{xx} \sim \rho$ is not allowed from the discussion in Section 1.2, so we must have $J_{xx} \sim \partial_x \rho$. This then gives $\partial_t \rho \sim \partial_x^2 J_{xx} = \partial_x^3 \rho$. The predicted behavior, $\partial_t \rho \sim \partial_x^3 \rho$, is then only visible by tracking an increasing octopole moment. When we say optimizing over the octopole moment, what are we explicitly doing? Let's assume we have some set, V , of orthonormal vectors that correspond to the preferred transitions described by the allowed f s, and let $\vec{A} \cdot \vec{V}_i$ represent the octopole moment of each motif with a non-zero f in V_i .

$$\vec{A} \cdot \vec{a} = 1^3 a_0 + 2^3 a_1 + \dots + (x+1)^3 a_x \quad (3.3.2)$$

where the a_i represent the individual charges in the a motif. We are looking for the corresponding c_i that maximizes $\vec{A} \cdot c_i \vec{V}_i$. The c_i values obey the constraint $\sum_i c_i^2 = 1$, and with this we can use Lagrange multipliers

to maximize c_i .

$$L = \vec{A} \cdot \vec{V}_i c_i - \frac{\lambda}{2}(c_i^2 - 1) \quad (3.3.3)$$

$$\frac{\partial L}{\partial c_i} = \vec{A} \cdot \vec{V}_i - \lambda c_i = 0 \quad (3.3.4)$$

$$c_i = \frac{\vec{A} \cdot \vec{V}_i}{\lambda} \quad (3.3.5)$$

$$= \frac{\vec{A} \cdot \vec{V}_i}{\sqrt{\sum_i (\vec{A} \cdot \vec{V}_i)^2}} \quad (3.3.6)$$

With this calculation we are looking at the normalized sum of the octopole moment of every state in the null vector block, and the largest sum will give us the largest signal when we simulate.

Chapter 4

Numerical Results

Now that we know the reasoning behind the algorithm, what results have we been able to produce?

4.1 Recovering previous results

We start by reproducing previous results from the literature. We are looking to recreate the dressed Gaussian[4] and the $z = 4$ sub-diffusion.

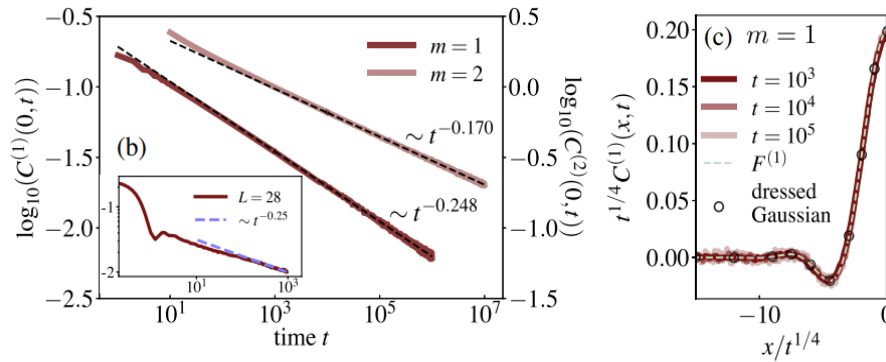


Figure 4.1: Results from previous literature [4]. b) is sub-diffusive results for $C(0, t)$ in dipole and quadrupole conserving fluids. c) shows scaling collapse according to the long wavelength description

In Figure 4.2 we see the predicted (1.2.4) $t \sim x^4$ scaling. The plots in Figure 4.1 and Figure 4.2 show a correlation function, which we track by calculating the correlation function $C(x, t) = \langle s(y, z)s(y+x, z+t) \rangle$, which is the average over all y, z of the product inside the brackets where $s(y, z)$ is the charge on some site y at time z . When we simulate the full $C(x, t)$ function we also see the predicted $C(x, t) = t^{-\frac{1}{z}} f(xt^{-\frac{1}{z}})$. The

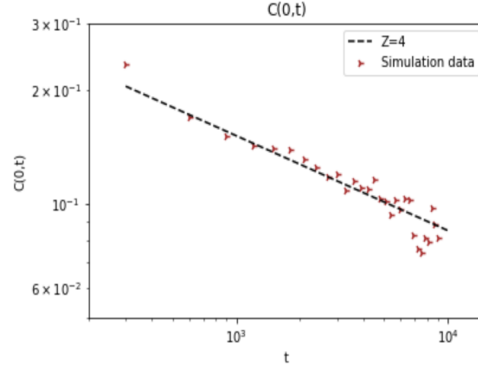


Figure 4.2: Simulation for $m = 3$, $q = 5$ showing $C(0, t)$ giving $Z = 4$ sub-diffusive behavior

predicted $f(xt^{-\frac{1}{Z}})$ is given by

$$f(xt^{-\frac{1}{4}}) = \int dx e^{-k^4 t} \cos kx \quad (4.1.1)$$

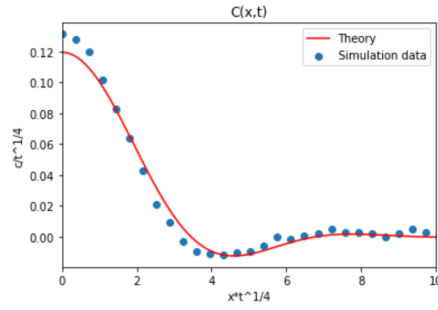


Figure 4.3: $C(x, t)$ correlation function following (4.1.1) and agreeing with Figure 4.1, finding the long wavelength description.

4.2 Towards breaking time-reversal symmetry

To explore why this behavior occurs, we need to be able to controllably break time-reversal symmetry, and we do this using the algorithm as described in Chapter 3. The first part of the algorithm finds the allowed motifs, for $m = q = 2$ we expect only 01 and 10 to be allowed.

$$\begin{bmatrix} 0.0 & -0.707106781186548 & 0.707106781186547 & 0.0 \end{bmatrix}$$

Figure 4.4: Null vector for $m = q = 2$, $n_{01} = -\frac{1}{\sqrt{2}}$, $n_{10} = \frac{1}{\sqrt{2}}$

We can read Figure 4.4 as giving the f value for the 00, 10, 01, 11 motifs respectively, and we see that the allowed motifs part of the algorithm gives the null vector we expect for small systems. Further, for $m = 2, q = 3$ with just charge conservation we expect to find $2^{3-1} - 1 = 3$ null vectors.

$$\begin{array}{c}
 \left[\begin{array}{ccc}
 [0 & 0 & 0] \\
 [0 & 0 & 1] \\
 [0 & 1 & 0] \\
 [0 & 1 & 1] \\
 [1 & 0 & 0] \\
 [1 & 0 & 1] \\
 [1 & 1 & 0] \\
 [1 & 1 & 1]
 \end{array} \right] \\
 \text{(a)}
 \end{array}
 \quad
 \begin{array}{c}
 \left[\begin{array}{ccc}
 0.0 & 0.0 & 0.0 \\
 -0.569343045498243 & 0.500000000026152 & 0.0958189662465586 \\
 -0.100845297849976 & -0.49999999997994 & 0.270489686246247 \\
 -0.367653794485758 & -0.499999999977861 & -0.445156799705694 \\
 0.670188343348219 & -2.81584037764332 \cdot 10^{-11} & -0.366308652492806 \\
 0.100843953257863 & 0.49999999997994 & -0.270486079685291 \\
 0.266809841227894 & -2.01329775033103 \cdot 10^{-11} & 0.715642879390985 \\
 0.0 & 0.0 & 0.0
 \end{array} \right] \\
 \text{(b)}
 \end{array}$$

Figure 4.5: a) Motifs corresponding to the vector entries. b) Null vectors for $m = 2, q = 3$. Each entry is the f value for the corresponding motif. Similarly to Figure 4.4, we can read the columns in (b) as the f values corresponding to the motif in the same row in (a). 001 can have an f value of -.596, .5 or .0958 etc.

In this figure, we can read the middle column as saying that $n_{001} + n_{101} = n_{010} + n_{011}$. The motifs 100 and 110 are also non-zero, and would complete the pattern of the LHS being a cycle of 001 and the RHS being a cycle of 101, but the value is so close to 0 that we'd need a larger run to be sure of the update rule. From this set of null vectors we can optimize over the octopole moment to find our transition rules.

$$\begin{array}{cccccccc}
 000 & 001 & 010 & 011 & 100 & 101 & 110 & 111 \\
 [0.0 & -.5963 & -.1008 & -.3677 & .6702 & .1008 & .2668 & 0]
 \end{array}$$

Figure 4.6: Optimized vector for $m = 2, q = 3$. Each f value is underneath it's corresponding motif, so 001 has an f of -.5963 etc.

Now that we can find the transition rules we can finally build the \mathcal{T} -breaking transition matrix. As a reminder, the \mathcal{T} -breaking transition matrix is a sum of the fully symmetric transition matrix and the fully \mathcal{T} -broken transition matrix. For $m = q = 2$ we expect Figure 2.3.1, and we produce 4.7.

The ordering of the rows is not the same as the example because the code hashes the states using $H = \sum_i^L q_i^i$ which calculates from the value of a binary string as 10 = 1 and 01 = 2. We see a uniform

$$\begin{bmatrix} 1.0 & 0 & 0 & 0 \\ 0 & 0.25 & 0.25 & 0 \\ 0 & 0.75 & 0.75 & 0 \\ 0 & 0 & 0 & 1.0 \end{bmatrix}$$

Figure 4.7: \mathcal{T} breaking transition matrix for $m = q = 2$, the columns are ordered 00, 10, 01, 11

stationary distribution by multiplying the matrix with $|1111\rangle$ and getting $|1111\rangle = \mathbf{Q}|1111\rangle$. To turn the optimal vector into the transition matrix, we create a dictionary with all possible values for the charge and dipole moment being the keys. The associated values are a tuple containing: the states belonging to the charge and dipole blocks and the f value the state is associated with. From there we iterate through each q -gate, comparing if the f value is positive or negative, and calculating the transition probability from states with positive f values to states with negative f values as described in Section 3.1. We add these transition probabilities to an empty matrix of size $m^q \times m^q$ where the index for each q -gate is the unique hash as given in the discussion above. To create the symmetric transition matrix we iterate through each charge and dipole block assigning $\mathbf{Q}_{ij} = \frac{1}{N}$ where N is the size of the block.

Unfortunately we were not able to do a large scale numerical simulation due to time constraints and errors in the main loop.

Chapter 5

Conclusion

The purpose of this thesis is to develop rigorous tools to probe new hydrodynamic universality classes and determine if it is stable to fluctuations? These are the questions posed at the start of this thesis, and while we have developed a framework to answer these questions, it remains to efficiently implement the algorithm numerically to find the $t \sim x^3$ scaling.

In particular, we developed an algorithm to provably and controllably break time-reversal symmetry in classical many-body Markov chains with charge and dipole conservation. This algorithm simulates a 3rd derivative drift term in the generalized (dipole-conserving) Fick's law and finds the preferred transitions that break detailed balance while maintaining charge and dipole conservation. From these update rules we are able to construct a Markov chain that preserves stationarity with a known stationary distribution, has update rules which are spatially local (on q sites), while breaking detailed balance.

All of this was programmed in Python, and future work will include running a full simulation for large m, q, L values to observe how the relaxation time scales with the system size, along with probing two-point correlation functions of the charge density, and any other valuable probes of hydrodynamic behavior that we develop.

Bibliography

- [1] Michael Crossley, Paolo Glorioso, and Hong Liu. Effective field theory of dissipative fluids. Journal of High Energy Physics, Sept 2017.
- [2] Suman G. Das, Abhishek Dhar, Keiji Saito, Christian B. Mendl, and Herbert Spohn. Numerical test of hydrodynamic fluctuation theory in the fermi-pasta-ulam chain. Physical Review E, 90(1), jul 2014.
- [3] Jan de Boer, Jelle Hartong, Niels Obers, Watse Sybesma, and Stefan Vandoren. Hydrodynamic modes of homogeneous and isotropic fluids. SciPost Physics, 5(2), aug 2018.
- [4] Johannes Feldmeier, Pablo Sala, Giuseppe De Tomasi, Frank Pollmann, and Michael Knap. Anomalous diffusion in dipole- and higher-moment-conserving systems. Phys. Rev. Lett., 125:245303, Dec 2020.
- [5] M. Giacinti Baschetti and M.G. De Angelis. 8 - vapour permeation modelling. In Angelo Basile, Alberto Figoli, and Mohamed Khayet, editors, Pervaporation, Vapour Permeation and Membrane Distillation, Woodhead Publishing Series in Energy, pages 203–246. Woodhead Publishing, Oxford, 2015.
- [6] Andrey Gromov, Andrew Lucas, and Rahul M. Nandkishore. Fracton hydrodynamics. Phys. Rev. Res., 2:033124, Jul 2020.
- [7] Elmer Guardado-Sanchez, Alan Morningstar, Benjamin M. Spar, Peter T. Brown, David A. Huse, and Waseem S. Bakr. Subdiffusion and heat transport in a tilted two-dimensional fermi-hubbard system. Phys. Rev. X, 10:011042, Feb 2020.
- [8] Jinkang Guo, Paolo Glorioso, and Andrew Lucas. Fracton hydrodynamics without time-reversal symmetry. Phys. Rev. Lett., 129:150603, Oct 2022.
- [9] Mehran Kardar, Giorgio Parisi, and Yi-Cheng Zhang. Dynamic scaling of growing interfaces. Phys. Rev. Lett., 56:889–892, Mar 1986.
- [10] Nikolaos D. Katopodes. Chapter 3 - diffusive mass transfer. In Nikolaos D. Katopodes, editor, Free-Surface Flow, pages 184–270. Butterworth-Heinemann, 2019.
- [11] David A. Levin and Yuval Peres. Markov Chains and Mixing Times: Second Edition. American Mathematical Society, 2017.
- [12] Andrew Lucas and Kin Chung Fong. Hydrodynamics of electrons in graphene. Journal of Physics: Condensed Matter, 30(5):053001, jan 2018.